Drawing Dispersion Curves: Band Structure Customization via Nonlocal Phononic Crystals

Arash Kazemi,[1,*] Kshiteej J. Deshmukh,[2,*] Fei Chen,[1,*] Yunya Liu,[1] Bolei Deng,[3,4] Henry Chien Fu,[1,†] and Pai Wang[1,‡]

[1]*Department of Mechanical Engineering, University of Utah, Salt Lake City, Utah 84112, USA*
[2]*Department of Mathematics, University of Utah, Salt Lake City, Utah 84112, USA*
[3]*Department of Electrical Engineering and Computer Science, Massachusetts Institute of Technology, Cambridge, Massachusetts 02139, USA*
[4]*Department of Mechanical Engineering, Massachusetts Institute of Technology, Cambridge, Massachusetts 02139, USA*

(Received 1 February 2023; accepted 13 September 2023; published 26 October 2023)

Dispersion relations govern wave behaviors, and tailoring them is a grand challenge in wave manipulation. We demonstrate the inverse design of phononic dispersion using nonlocal interactions on one-dimensional spring-mass chains. For both single-band and double-band cases, we can achieve any valid dispersion curves with analytical precision. We further employ our method to design phononic crystals with multiple ordinary (roton or maxon) and higher-order (undulation) critical points and investigate their wave packet dynamics.

DOI: 10.1103/PhysRevLett.131.176101

Phononic crystals and vibroelastic metamaterials are architected heterogeneous solids for the manipulation of mechanical waves. They can exhibit many unconventional properties, such as frequency band gaps [1–7], negative refraction [8–11], and topologically protected modes [12–15]. They also have a wide range of applications in cloaking [16–20], signal manipulation [21,22], focusing [23,24], and energy trapping [25–27]. Recently, by incorporating nonlocal (i.e., farther than nearest neighbor) interactions [28], Rosa and Ruzzene [29–32] demonstrated diffusive transport, and Wu and Huang [33,34] investigated active control, while Chen *et al.* [35] showed rotonlike dispersion [36–42], where the local minimum of the dispersion curve resembles the roton behavior [43–45] of the helium-4 superfluid [46–50] at low temperature. All these exotic and desirable dynamic behaviors hinge on the dispersion relation—how frequency depends on wave vector—that is intrinsic to each particular design. However, most studies so far have been focused on the forward problem from a given design to a set of band structures. It is a long-standing goal in the research community to solve the inverse problem from given dispersion bands to actual metamaterial designs so that exotic behaviors and functionalities can be realized on demand. Prior efforts to tailor specific dispersions [51–55] or band gaps [56–59] typically relied on iterative searches with high computational costs, and they had only very limited success.

In this Letter, we demonstrate a design methodology that uses nonlocal interactions to customize dispersion relations. First, we present an analytical protocol to solve the inverse problem, achieving any arbitrarily defined single-band dispersion on monoatomic nonlocal chains. Then, we use this design protocol to obtain dispersion curves with ordinary and higher-order critical points. Using time-domain simulations, we illustrate their unconventional wave dynamics, especially at the undulation point (also known as stationary inflection point), where both the first and second derivatives of the dispersion curve vanish. This results in highly concentrated vibration energy since the wave mode is simultaneously nonpropagating and nonspreading. Finally, we also investigate the diatomic nonlocal chain and develop the design protocol to customize its two dispersion bands.

We start with a one-dimensional "monoatomic" phonon chain of identical masses, m, and linear springs. A schematic of the model is depicted in Fig. 1(a). Each mass

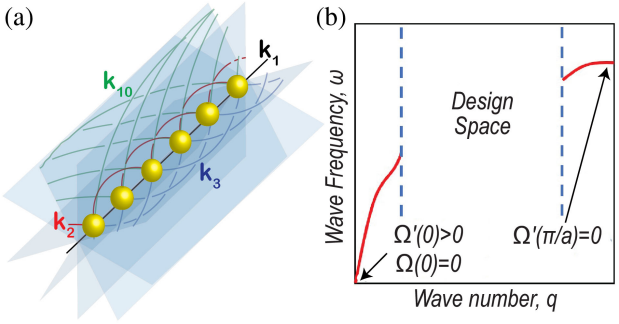

FIG. 1. (a) An infinite chain of identical masses. Each mass is connected to its nth-nearest neighbors with spring constant k_n. (b) The design space with fundamental constraints at the center ($q = 0$) and edge ($q = \pi/a$) of the first Brillouin zone.

is connected with its two nearest neighbors by local interactions with the spring constant k_1. In addition, each mass is also connected on both sides to its two nth-nearest neighbors with nonlocal interactions specified by the spring constants k_n, for $n = 2, 3, 4, \ldots, N$, where N is the longest-range nonlocal interaction in the system. The governing equation of motion for the jth mass is

$$m\ddot{u}_j = \sum_{n=1}^{N} k_n(u_{j+n} - 2u_j + u_{j-n}). \tag{1}$$

Based on the Bloch theorem [60], we obtain the following dispersion relation:

$$\omega^2(q) = \frac{2}{m}\left(\sum_{n=1}^{N} k_n - \sum_{n=1}^{N} k_n \cos(nqa)\right), \tag{2}$$

where ω is the frequency, q is the wave number, and a is the spatial period of the lattice. For conventional chains with local springs k_1 only, Eq. (2) reduces to the classical result of $\omega^2(q) = (4k_1/m)\sin^2(qa/2)$, which is always monotonic and reaches its maximum at the Brillouin zone boundary [61]. The nonlocal interactions, on the other hand, may give rise to local minima and maxima at the interior of the Brillouin zone, as recently demonstrated by Chen *et al.* [35] and earlier by Farzbod and Leamy [62].

Since Eq. (2) takes the form of a Fourier series, we can use it to tailor the nonlocal interactions to achieve any desirable dispersion behavior. Mathematically, this originates from the fact that the dynamic matrix or Hamiltonian takes the form of a circulant matrix. Before the demonstration of customization procedures, it is necessary to understand all constraints in possible dispersion relations. Here, we consider the following physical and symmetry principles as fundamental assumptions of the designer nonlocal phononic crystals: (i) passive with no energy input or output, (ii) freestanding with no grounded springs, (iii) time-reversal symmetric with no gyroscopic effect, and (iv) stable with a finite static stiffness.

Combining the above, we arrive at the requirements that, for any target dispersion relation $\Omega(q)$ defined on the non-negative half of the first Brillouin zone ($q \in [0, \pi/a]$) to be valid, it needs to be a smooth curve with [See Fig. 1(b)]:

$$\Omega(0) = 0, \quad 0 < \Omega'(0) < +\infty, \quad \text{and} \quad \Omega'(\pi/a) = 0. \tag{3}$$

Given an arbitrarily specified dispersion relation, $\Omega(q)$, satisfying Eqs. (3), we can design a nonlocal phononic crystal using the following protocol. First, we find the Fourier coefficients as

$$A_n = \frac{2a}{\pi}\int_0^{\pi/a} \Omega^2(q)\cos(nqa)dq, \quad n = 1, 2, \ldots, N. \tag{4}$$

Then, the design can be obtained by

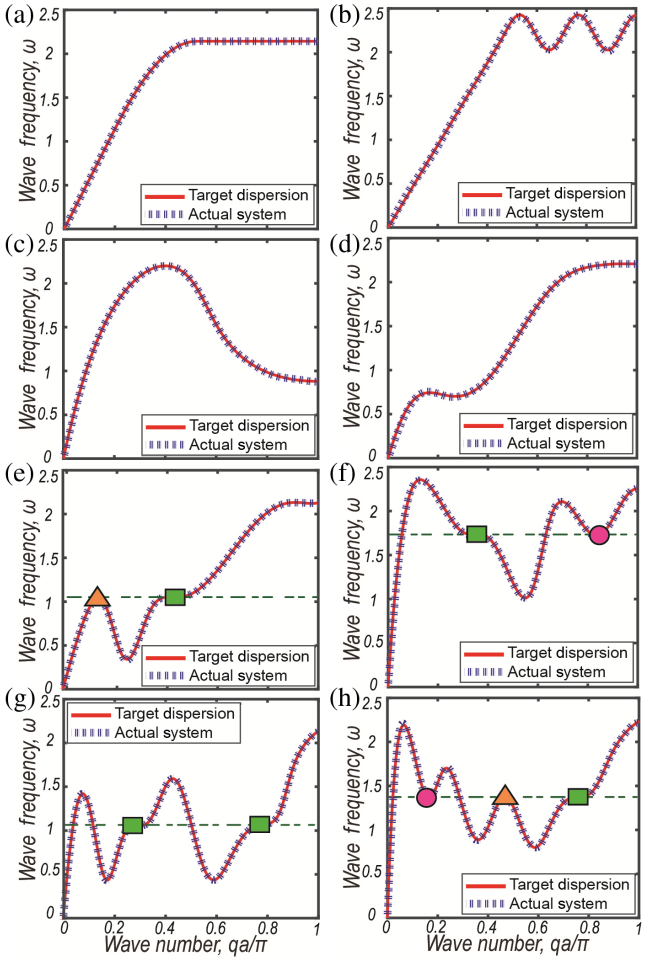

FIG. 2. Customized dispersion curves with special features.: (a) a flattop; (b)–(d) nonmonotonic behaviors at large, medium, and small wave number q (i.e., at short, medium, and long wavelength as compared to unit cell size), respectively; (e)–(h) undulation points (squares), maxons (triangles), and rotons (circles) occurring at the same frequency.

$$k_n/m = -A_n/2, \qquad n = 1, 2, \ldots, N. \tag{5}$$

Figure 2 shows results of this protocol with several examples. Since Eq. (5) shows all k_ns simply scale with m, we can set $m = 1$ for all cases. In each case, we compare the target dispersion with the actual one by examining the normalized root mean square deviation (NRMSD) between them. We purposefully choose the target curves with various interesting features. In the implementation, we use analytical functions as the targets for Figs. 2(a) and 2(b). For other cases, we use piecewise spline functions to construct target curves. The detailed procedures are given in the Supplemental Material [63]. For each target curve, the stiffness design variables are obtained using Eqs. (4) and (5). The total number of stiffness types is $N = 10$ for Figs. 2(a)–2(d), $N = 20$ for Figs. 2(e)–2(g), and $N = 25$ for Fig. 2(h), respectively.

The NRMSD is less than 1% in all cases, and the details are given in the Supplemental Materials [63]. We show that it is possible to achieve a flat band top [Fig. 2(a)] as well as nonmonotonic dispersion at relatively short [Fig. 2(b)], medium [Fig. 2(c)], and long [Fig. 2(d)] wavelength regimes. In addition, for critical points on the dispersion, we can design systems where local maxima (maxons), local minima (rotons), and stationary inflection points (undulations) can occur at the same frequency, as illustrated in Figs. 2(e) and 2(f).

Next, we investigate these critical points that exhibit exotic dynamics by considering two specific instances of nonlocal phononic crystals with the third-nearest-neighbor (k_3) interactions as the only nonlocal effect. When, $k_3 = 3k_1$ [Fig. 3(a), top], the dispersion curve is nonmonotonic [blue solid curve in Fig. 3(b)], exhibiting one local maximum (maxonlike) and one local minimum (rotonlike [35]) at $qa = 2\tan^{-1}(\sqrt{(11/7) \pm (6\sqrt{2}/7)})$. Both of them represent critical-point wave modes with zero group velocity (ZGV), and they are analogous to the Van Hove singularities [68] in electronic band structures. These ZGV modes also have promising applications in many wave-related engineering technologies such as noninvasive structural health monitoring [69–72] since the highly localized wave modes can enhance both the vibration energy concentration and the signal-to-noise ratio in ultrasonic probing. In contrast, when $k_3 = k_1/3$ [Fig. 3(a), bottom], the dispersion curve is monotonic [black dotted curve in Fig. 3(b)] with an undulation point in the middle at $qa = \pi/2$, where both the first and second derivatives vanish. While rotonlike dispersions were recently demonstrated [35–41], and undulation points of electromagnetic waves in optical waveguides were studied as frozen modes [73–75], we show here, for the first time, a second-order-critical undulation point for vibroelastic waves in phononic crystals.

To demonstrate wave behaviors at these critical points, we also perform two types of time-domain simulations on finite chains.

First, we apply a force excitation on the leftmost mass of a chain with 5000 unit cells. The forcing function is a Gaussian envelope in time:

$$f(t) = \exp\left[-(t - t_m)^2/\tau^2\right]\cos\left(\omega_c t\right), \tag{6}$$

where ω_c is the carrier frequency corresponding to the critical point, t_m is the peak time of the envelope, and $\tau = 100/\omega_c$ characterizes the time duration of the envelope. Figures 3(c) and 3(d) show the results for maxonlike and rotonlike dynamics, respectively, in the chain with $k_3 = 3k_1$. In each case, two modes of the same frequency but different wavelengths are observed: one is the traveling mode [hollow triangle and circle in [Fig. 3(b)] with finite group velocity, as indicated by the black dashed line, while the other is the ZGV mode [filled triangle and circle in Fig. 3(b)] localized at the source. Although the maxonlike and rotonlike ZGV modes are not traveling waves, the results show they do diffuse and spread out in space over time. In contrast, Fig. 3(e) shows the result at the undulation-point frequency on the chain with $k_3 = k_1/3$. Only one wave mode is observed. More importantly, not only is this mode nonpropagating, but it is also nonspreading, as both the group velocity, $\omega'(q)$, and the diffusion rate, $\omega''(q)$, vanish. This is a unique feature that does not exist in ordinary ZGV modes.

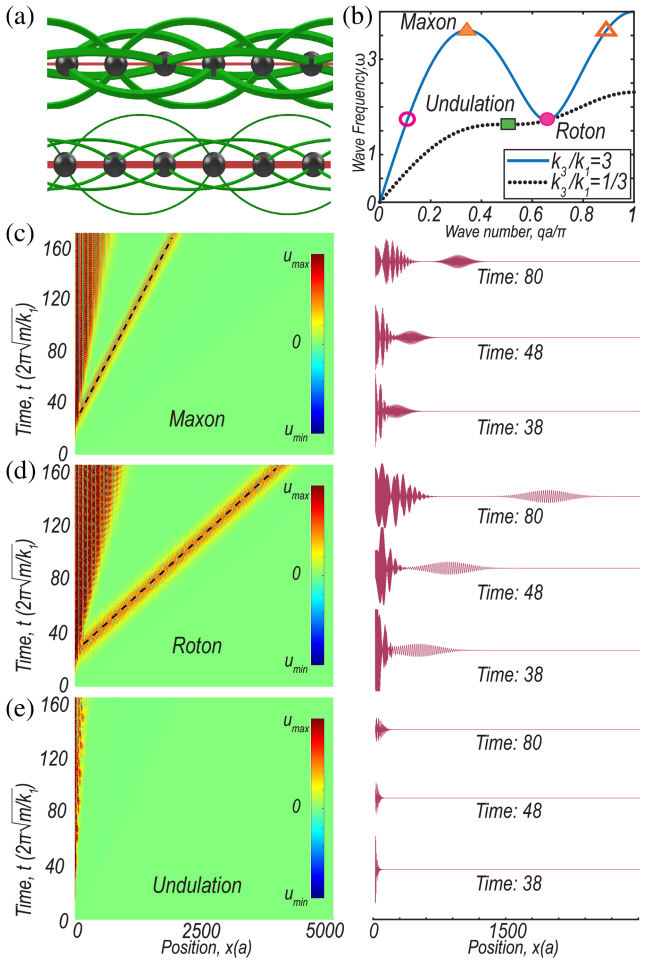

FIG. 3. (a) Schematics of two nonlocal phononic crystals with the first and third nearest-neighbor interactions only—top, $k_3 = 3k_1$; bottom, $k_3 = k_1/3$. (b) Dispersion curves. For $k_3 = 3k_1$, a local maximum (maxon) appears at $(\omega, qa/\pi) = (3.61, 0.344)$, and a local minimum (roton) appears at $(\omega, qa/\pi) = (1.72, 0.656)$. For $k_3 = k_1/3$, a stationary inflection point (undulation) appears at $(\omega, qa/\pi) = (1.63, 0.5)$, where both the first and second derivatives vanish. (c)–(e) Time-domain results for the 3 critical points in (b): maxon, roton, and undulation, respectively. The left column lists the time-space plots, while the right column shows wave amplitude snapshots.

Second, to further investigate the diffusion phenomena, we look into the time evolution of a localized Gaussian spatial wave packet,

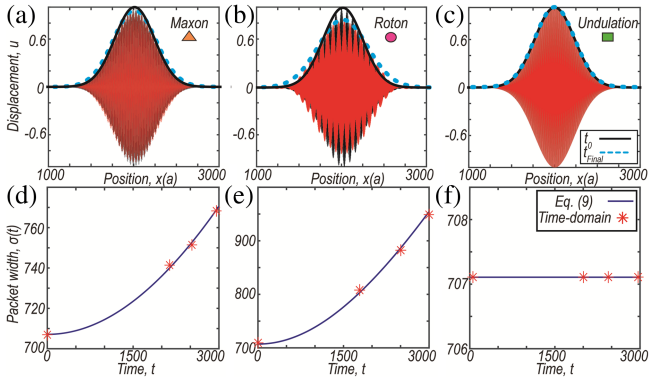

FIG. 4. Diffusion at the critical points. Evolution of an initially prescribed Gaussian packet with different carrier wave number q (i.e., different carrier wavelength) corresponding to the critical points in Fig. 3(b): (a) maxon mode with $qa/\pi = 0.656$, (b) roton mode with $qa/\pi = 0.344$, (c) undulation mode with $qa/\pi = 0.5$. The Gaussian envelope at time t_{Final} (blue dotted curve) is compared to the initial envelope at t_0 (black solid curve). (d)–(f) Theoretical and numerical values of $\sigma(t)$ vs t for each of the cases in (a)–(c), respectively, showing the spreading of wave envelopes.

$$u(x,t) = \exp\left[-(x-x_0)^2/\sigma(t)\right]\cos q_c x, \tag{7}$$

where q_c is the carrier wave number corresponding to the critical point, x_0 denotes the center of the wave packet, and $\sigma(t)$ characterizes the width of the envelope. We prescribe an initial Gaussian packet with $\sigma(t=0) = \sigma_0$. In each case, there is only one wave mode associated with the prescribed wave number q_c corresponding to the critical point, and it is a ZGV mode. As such, the wave packet does not propagate. However, the wave packet can still spread out or diffuse in space, i.e., while maintaining the same mean x_0, the envelope width $\sigma(t)$ changes, and its evolution over time is governed by [76]

$$\sigma(t) = \sigma_0\sqrt{1 + (t\omega''/\sigma_0^2)^2}. \tag{8}$$

Numerically, we can determine the diffusion rate of the wave packet by tracking $\sigma(t)$ in time-domain simulations on finite chains. Figures 4(a)–4(c) show the comparison of wave packet diffusion for the three critical points: local maximum (maxonlike), local minimum (rotonlike), and the undulation point (second order), respectively. In each case, the initial ($t = 0$) wave envelope is represented by a black solid line. After evolving for sufficient time ($t = t_{\mathrm{Final}}$) the resulting wave envelope is shown as a blue dotted line. Figures 4(d)–4(f) show, for each of the cases in Figs. 4(a)–4(c), respectively, the evolution of the packet width, $\sigma(t)$, at several time instances. Broadening of the envelope is observed for both maxon and roton packets, where $\omega' = 0$ but $\omega'' \neq 0$. In contrast, the wave envelope preserves its initial shape without diffusion in the case of the undulation point, where $\omega'' = \omega' = 0$. Lastly, we also establish the customization protocol for the double-band system of a one-dimensional "diatomic" nonlocal phononic chain consisting of two different masses m_1 and m_2. This model leads to the following dispersion relations:

$$\omega_\pm^2 = K_0\left(\frac{1}{m_1}+\frac{1}{m_2}\right) \mp \sqrt{K_0^2\left(\frac{1}{m_1}+\frac{1}{m_2}\right)^2 + \frac{1}{m_1 m_2}(K_1^2 - 4K_0^2)}, \tag{9}$$

where $-$ and $+$ in the $\mp$ sign denote the first and second bands (historically referred to as "acoustic" and "optical" branches), respectively. Here, K_0 and K_1 are

$$K_0(q) = \sum_{n=1}^{N} k_n - \sum_{\substack{n=2 \\ n\ \mathrm{even}}}^{N} k_n \cos(nqa),$$
$$K_1(q) = 2\sum_{\substack{n=1 \\ n\ \mathrm{odd}}}^{N} k_n \cos(nqa), \tag{10}$$

which are defined on the non-negative half of the first Brillouin zone, $q \in [0, \pi/(2a)]$. Given two arbitrarily specified smooth curves as the targets, $\Omega_-(q)$ and $\Omega_+(q)$, satisfying all fundamental and symmetry requirements detailed in the Supplemental Material [63], we can design a nonlocal chain using the following protocol. First, we calculate

$$\alpha = m_2/m_1 = \Omega_+^2\left(\frac{\pi}{2a}\right)/\Omega_-^2\left(\frac{\pi}{2a}\right),$$
$$A(q) = [\Omega_+^2(q) + \Omega_-^2(q)]/2,$$
$$D(q) = [\Omega_+^2(q) - \Omega_-^2(q)]/2. \tag{11}$$

Then, we can get

$$K_0(q) = \alpha A(q)/(\alpha+1),$$
$$K_1^2(q) = 4K_0^2(q) - \alpha A^2(q) + \alpha D^2(q). \tag{12}$$

Lastly, we obtain the stiffness values as

$$k_n = \frac{2a}{\pi}\int_0^{\frac{\pi}{2a}} K_1 \cos(naq)dq, \qquad n = 1,3,5,\ldots$$
$$k_n = -\frac{4a}{\pi}\int_0^{\frac{\pi}{2a}} K_0 \cos(naq)dq, \qquad n = 2,4,6,\ldots \tag{13}$$

We note that the above protocol is capable of customizing each individual band without affecting the other since it can work for two independently defined targets, $\Omega_-(q)$ and $\Omega_+(q)$. Figures 5(a)–5(d) show the results of this protocol by setting $m_1 = 1$. The target curves are purposefully chosen with various features: Fig. 5(a) demonstrates a rising first band with a flat second band; Fig. 5(b) shows

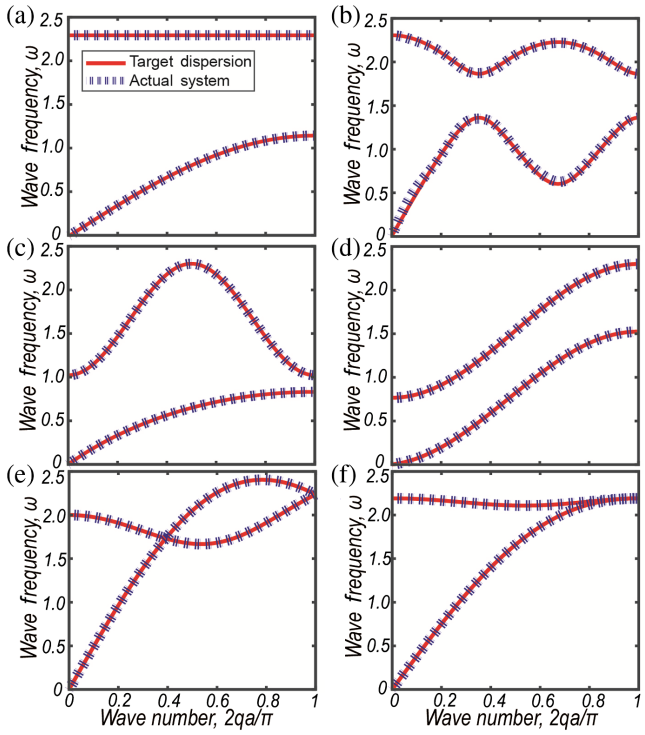

FIG. 5. (a)–(d) Customized double-band dispersion relations. black (e) and (f) show examples with linear (Dirac-like) and quadratic band crossings, respectively.

two bands with changing but always opposite convexity; Fig. 5(c) has a constant-curvature first band and an arched second band; and Fig. 5(d) has both bands monotonically increasing. These examples show that both localized and traveling wave modes can be designed at any arbitrarily desirable frequency and wavelength by our protocol on either band. In the implementation, we set the total number of stiffness types as $N = 20$ for Fig. 5. We also examine NRMSD values between the target and actual dispersion curves. The results show that, in most cases, a good match can be achieved with just a small number of nonlocal springs. Furthermore, we also demonstrate the protocol's capability of realizing linear (Dirac-cone-like) and quadratic band crossings in Figs. 5(e) and 5(f), respectively. Detailed information and additional examples are presented in the Supplemental Material [63].

In conclusion, we can completely and analytically customize the dispersion relations in phononic crystals by incorporating nonlocal springs. We show dispersion curves with multiple critical points of the first (maxon and roton) and second order (undulation). We further study the wave packet dynamics at each of the critical points and illustrate how we can use them to create novel behaviors of localized modes. This enables future research on higher-order critical points of elastic waves in terms of topology, scaling, and symmetry [77,78] in 2D and 3D systems. Finally, we can also solve the inverse problem for arbitrary two-band dispersion relations.

For practical considerations, physical samples of phononic metamaterials with a small number of nonlocal springs can be fabricated in relatively simple designs [38,41,79]. In fact, one-dimensional chains with any number of nonlocal connections are, at least in principle, feasible by the following reasoning: There are infinitely many planes that contain the line of masses. Hence, each nonlocal interaction can exist in a separate plane without interfering with others, similar to the design illustrations shown in Figs. 1(a) and 3(a), and in more detail in the Supplemental Material [63]. During the review process, we became aware of recent experimental efforts demonstrating nonlocal effects [80–83]. They provide further evidence supporting feasibility in design and fabrication. We are confident that future research efforts will enable more sophisticated experimental setups with many more nonlocal interactions in 2D and 3D phononic crystals and vibroelastic metamaterials.

At the continuum limit of the lattice constant $a \to 0$, wave mechanics in nonlocal continuum media can be described by higher-order strain-gradient models [84–86] as well as *peridynamics* [87,88]. In contrast to those popular phenomenological and semiphenomenological approaches, our method has the advantage of prescribing system parameters to achieve desirable dynamic behaviors. Homogenizing our design methodology could potentially provide a route to design the micromodulus elasticity kernel for target dispersion relations in continuum vibroelastic metamaterials.

This work was supported by the P. W.'s startup research funds of the Department of Mechanical Engineering at University of Utah. K. J. D. is grateful to the National Science Foundation for support through Grant No. DMS-2107926. The support and resources from the Center for High Performance Computing at the University of Utah are gratefully acknowledged. The authors are grateful to Professor Graeme Milton at Utah, Professor Srikantha Phani at UBC, Professor Mahmoud Hussein at CU Boulder, and Professor Guancong Ma at HKBU for inspirational discussions.

*These authors contributed equally to this work.
†Corresponding author: henry.fu@utah.edu
‡Corresponding author: pai.wang@utah.edu

[1] Z. Liu, X. Zhang, Y. Mao, Y. Zhu, Z. Yang, C. T. Chan, and P. Sheng, Science **289**, 1734 (2000).
[2] P. Wang, F. Casadei, S. H. Kang, and K. Bertoldi, Phys. Rev. B **91**, 020103(R) (2015).
[3] S. G. Konarski, C. J. Naify, and C. A. Rohde, Appl. Phys. Lett. **116**, 051903 (2020).
[4] C. L. Willey, V. W. Chen, D. Roca, A. Kianfar, M. I. Hussein, and A. T. Juhl, Phys. Rev. Appl. **18**, 014035 (2022).
[5] I. Arretche and K. H. Matlack, J. Sound Vib. **540**, 117305 (2022).

[6] C. Widstrand, N. Kalantar, and S. Gonella, Extreme Mech. Lett. **53**, 101693 (2022).
[7] W. Ding, T. Chen, C. Chen, D. Chronopoulos, J. Zhu, and B. Assouar, Mech. Syst. Signal Process. **186**, 109922 (2023).
[8] N. Kaina, F. Lemoult, M. Fink, and G. Lerosey, Nature (London) **525**, 77 (2015).
[9] L. Fang and M. J. Leamy, *International Design Engineering Technical Conferences and Computers and Information in Engineering Conference* (American Society of Mechanical Engineers, 2021), 10.1115/DETC2021-71840.
[10] H. Danawe and S. Tol, J. Sound Vib. **518**, 116552 (2022).
[11] L. Fang and M. Leamy, J. Acoust. Soc. Am. **151**, A39 (2022).
[12] P. Wang, L. Lu, and K. Bertoldi, Phys. Rev. Lett. **115**, 104302 (2015).
[13] H. Danawe, H. Li, K. Sun, and S. Tol, Phys. Rev. Lett. **129**, 204302 (2022).
[14] K. Ding, C. Fang, and G. Ma, Nat. Rev. Phys. **4**, 745 (2022).
[15] M. Charara, J. McInerney, K. Sun, X. Mao, and S. Gonella, Proc. Natl. Acad. Sci. U.S.A. **119**, e2208051119 (2022).
[16] S. A. Cummer and D. Schurig, New J. Phys. **9**, 45 (2007).
[17] H. Nassar, Y. Y. Chen, and G. L. Huang, Phys. Rev. Lett. **124**, 084301 (2020).
[18] X. Xu, C. Wang, W. Shou, Z. Du, Y. Chen, B. Li, W. Matusik, N. Hussein, and G. Huang, Phys. Rev. Lett. **124**, 114301 (2020).
[19] F. Martinez and M. Maldovan, Mater. Today Phys. **27**, 100819 (2022).
[20] C. Xu, K. Lyu, and Y. Wu, Europhys. Lett. **141**, 15002 (2022).
[21] P. Karki and J. Paulose, Phys. Rev. Appl. **15**, 034083 (2021).
[22] N. Kruss and J. Paulose, Phys. Rev. Appl. **17**, 024020 (2022).
[23] C. Xu, G. Okudan, H. Danawe, D. Ozevin, and S. Tol, *Nondestructive Characterization and Monitoring of Advanced Materials, Aerospace, Civil Infrastructure, and Transportation XVI* (SPIE, 2022), pp. 189–196, 10.1117/12.2612906.
[24] G. Okudan, C. Xu, H. Danawe, S. Tol, and D. Ozevin, *Improved Detection of Localized Damage in Pipe-Like Structures Using Gradient-Index Phononic Crystal Lens* (Springer International Publishing,, Cham, 2022), 10.1007/978-3-031-07322-9_30.
[25] J. M. De Ponti, A. Colombi, E. Riva, R. Ardito, F. Braghin, A. Corigliano, and R. V. Craster, Appl. Phys. Lett. **117**, 143902 (2020).
[26] M. Alshaqaq, C. Sugino, and A. Erturk, Phys. Rev. Appl. **17**, L021003 (2022).
[27] J. E. Pechac and M. J. Frazier, Appl. Phys. Lett. **122**, 211702 (2023).
[28] R. Fleury, Nat. Phys. **17**, 766 (2021).
[29] M. I. Rosa and M. Ruzzene, New J. Phys. **22**, 053004 (2020).
[30] M. Nora Rosa and M. Ruzzene, F25.00013: Dynamics and Topology of Non-Hermitian Elastic Lattices with Non-Local Feedback Interactions (2020), https://meetings.aps.org/Meeting/MAR20/Session/F25.13.
[31] M. I. Rosa and M. Ruzzene, New J. Phys. **24**, 073020 (2022).
[32] M. I. N. Rosa and M. Ruzzene, *Proc. SPIE PC12048, Health Monitoring of Structural and Biological Systems XVI* (2022).
[33] Q. Wu and G. Huang, ASME Int. Mech. Eng. Congr. Expo. **85543**, V001T01A015 (2021).
[34] Q. Wu, P. Shivashankar, X. Xu, Y. Chen, and G. Huang, J. Compos. Mater. **57**, 771 (2023).
[35] Y. Chen, M. Kadic, and M. Wegener, Nat. Commun. **12**, 3278 (2021).
[36] C. Prada, D. Clorennec, and D. Royer, J. Acoust. Soc. Am. **124**, 203 (2008).
[37] H. Godfrin, M. Meschke, H.-J. Lauter, A. Sultan, H. M. Böhm, E. Krotscheck, and M. Panholzer, Nature (London) **483**, 576 (2012).
[38] J. A. Iglesias Martínez, M. F. Groß, Y. Chen, T. Frenzel, V. Laude, M. Kadic, and M. Wegener, Sci. Adv. **7**, eabm2189 (2021).
[39] J.-N. Schmidt, J. Hertkorn, M. Guo, F. Böttcher, M. Schmidt, K. S. H. Ng, S. D. Graham, T. Langen, M. Zwierlein, and T. Pfau, Phys. Rev. Lett. **126**, 193002 (2021).
[40] H. Lyu, Y. Zhang, and T. Busch, Phys. Rev. A **106**, 013302 (2022).
[41] K. Wang, Y. Chen, M. Kadic, C. Wang, and M. Wegener, Commun. Mater. **3**, 75 (2022).
[42] Y. Chen, M. A. Abouelatta, K. Wang, M. Kadic, and M. Wegener, Adv. Mater. **35**, 2209988 (2023).
[43] L. Landau, Phys. Rev. **60**, 356 (1941).
[44] E. B. Kolomeisky, J. Colen, and J. P. Straley, Phys. Rev. B **105**, 054509 (2022).
[45] L. Chomaz, R. M. van Bijnen, D. Petter, G. Faraoni, S. Baier, J. H. Becher, M. J. Mark, F. Waechtler, L. Santos, and F. Ferlaino, Nat. Phys. **14**, 442 (2018).
[46] R. P. Feynman, Phys. Rev. **94**, 262 (1954).
[47] D. Henshaw and A. Woods, Phys. Rev. **121**, 1266 (1961).
[48] M. S. Bryan and P. E. Sokol, Phys. Rev. B **97**, 184511 (2018).
[49] H. Godfrin, K. Beauvois, A. Sultan, E. Krotscheck, J. Dawidowski, B. Fåk, and J. Ollivier, Phys. Rev. B **103**, 104516 (2021).
[50] N. P. Müller and G. Krstulovic, Phys. Rev. B **105**, 014515 (2022).
[51] H. Goh and L. F. Kallivokas, J. Eng. Mech. **145**, 04019094 (2019).
[52] H.-W. Dong, C. Shen, S.-D. Zhao, W. Qiu, H. Zheng, C. Zhang, S. A. Cummer, Y.-S. Wang, D. Fang, and L. Cheng, Natl. Sci. Rev. **9**, nwac030 (2022).
[53] W. Jiang, Y. Zhu, G. Yin, H. Lu, L. Xie, and M. Yin, Mater. Today Phys. **22**, 100616 (2022).
[54] Z. Wang, J. Du, W. Shen, J. Liu, and Z. He, Sensors **21**, 6651 (2021).
[55] N. Arora, Q. Yao, and S. Rudykh, Extreme Mech. Lett. **51**, 101592 (2022).
[56] E. B. Isaacs and C. Wolverton, Chem. Mater. **30**, 1540 (2018).
[57] H. Goh and L. F. Kallivokas, Wave Motion **88**, 85 (2019).
[58] H. Goh and L. F. Kallivokas, Comput. Methods Appl. Mech. Eng. **370**, 113263 (2020).
[59] J. Morris, W. Wang, D. Shah, T. Plaisted, C. J. Hansen, and A. V. Amirkhizi, Mater. Des. **216**, 110510 (2022).

[60] M. I. Hussein, M. J. Leamy, and M. Ruzzene, Appl. Mech. Rev. **66**, 040802 (2014).
[61] A. S. Phani, Dyn. Lattice Mater. **1**, 53 (2017).
[62] F. Farzbod and M. J. Leamy, J. Vib. Acoust. **133**, 031010 (2011).
[63] See Supplemental Material at http://link.aps.org/supplemental/10.1103/PhysRevLett.131.176101 for additional results, detailed derivations, and calculation procedures, which includes Refs. [64–67].
[64] J. Mei, Y. Wu, C. T. Chan, and Z.-Q. Zhang, Phys. Rev. B **86**, 035141 (2012).
[65] A. Maznev, J. Acoust. Soc. Am. **135**, 577 (2014).
[66] M. Lanoy, F. Lemoult, A. Eddi, and C. Prada, Proc. Natl. Acad. Sci. U.S.A. **117**, 30186 (2020).
[67] C. Xu, G. Ma, Z.-G. Chen, J. Luo, J. Shi, Y. Lai, and Y. Wu, Phys. Rev. Lett. **124**, 074501 (2020).
[68] L. Van Hove, Phys. Rev. **89**, 1189 (1953).
[69] O. Balogun, T. W. Murray, and C. Prada, J. Appl. Phys. **102**, 064914 (2007).
[70] J. Laurent, D. Royer, T. Hussain, F. Ahmad, and C. Prada, J. Acoust. Soc. Am. **137**, 3325 (2015).
[71] A. Geslain, S. Raetz, M. Hiraiwa, M. Abi Ghanem, S. Wallen, A. Khanolkar, N. Boechler, J. Laurent, C. Prada, and A. Duclos, J. Appl. Phys. **120**, 135107 (2016).
[72] Y. Wu, R. Cui, K. Zhang, X. Zhu, and J. S. Popovics, NDT & E Int. **132**, 102727 (2022).
[73] H. Ramezani, S. Kalish, I. Vitebskiy, and T. Kottos, Phys. Rev. Lett. **112**, 043904 (2014).
[74] H. Li, I. Vitebskiy, and T. Kottos, Phys. Rev. B **96**, 180301(R) (2017).
[75] A. Herrero-Parareda, I. Vitebskiy, J. Scheuer, and F. Capolino, Adv. Photonics Res. **3**, 2100377 (2022).
[76] M. Remoissenet, *Waves Called Solitons: Concepts and Experiments* (Springer Berlin, Heidelberg, 2013), 10.1007/978-3-662-03790-4.
[77] N. F. Q. Yuan and L. Fu, Phys. Rev. B **101**, 125120 (2020).
[78] A. Chandrasekaran, A. Shtyk, J. J. Betouras, and C. Chamon, Phys. Rev. Res. **2**, 013355 (2020).
[79] Z. Zhu, Z. Gao, G.-G. Liu, Y. Ge, Y. Wang, X. Xi, B. Yan, F. Chen, P. P. Shum, H.-x. Sun *et al.*, New J. Phys. **24**, 123019 (2022).
[80] G. J. Chaplain, I. R. Hooper, A. P. Hibbins, and T. A. Starkey, Phys. Rev. Appl. **19**, 044061 (2023).
[81] D. B. Moore, J. R. Sambles, A. P. Hibbins, T. A. Starkey, and G. J. Chaplain, Phys. Rev. B **107**, 144110 (2023).
[82] A. Bossart and R. Fleury, Phys. Rev. Lett. **130**, 207201 (2023).
[83] A. R. Alisepahi, K. Sun, and J. Ma, arXiv:2304.04080.
[84] H. Askes, A. V. Metrikine, A. V. Pichugin, and T. Bennett, Philos. Mag. **88**, 3415 (2008).
[85] K. Deshmukh, T. Breitzman, and K. Dayal, J. Mech. Phys. Solids **167**, 104992 (2022).
[86] B. Wang, J. Liu, A. Soh, and N. Liang, Appl. Math. Mech. **43**, 1 (2022).
[87] S. A. Silling, J. Mech. Phys. Solids **48**, 175 (2000).
[88] S. A. Silling and R. B. Lehoucq, Adv. Appl. Mech. **44**, 73 (2010).

Supplemental Material

to

Drawing Dispersion Curves – Band Structure Customization via Non-Local Phononic Crystals

Arash Kazemi*, [1]Kshiteej Deshmukh*, [2]Fei Chen*, [1]Yunya Liu,[1] Bolei Deng,[3,4] Henry Chien Fu,[1] and Pai Wang[1]

[1]*Department of Mechanical Engineering, University of Utah, Salt Lake City, UT, USA*

[2]*Department of Mathematics, University of Utah, Salt Lake City, UT, USA*

[3]*Department of Electrical Engineering and Computer Science, Massachusetts Institute of Technology, Cambridge, MA 02139, USA*

[4]*Department of Mechanical Engineering, Massachusetts Institute of Technology, Cambridge, MA 02139, USA*

CONTENTS

SYMMETRY AND PHYSICAL REQUIREMENTS OF SINGLE-BAND SYSTEM

Here we discuss the conditions of the valid dispersion curve for a passive, free-standing, and periodic mono-atomic spring-mass chain. First, every dispersion relation needs to obey the periodicity in the wave number q-space:

$$\omega(q) = \omega(q + 2\pi/a) \tag{S1}$$

where ω, q, and a denote (angular) frequency, (angular) wave number, and lattice constant, respectively. Besides, ordinary passive systems should all satisfy the time-reversal symmetry (See e.g. Joannopoulos et al. *Photonic Crystals: Molding the Flow of Light*. 2nd ed.):

$$\omega(-q) = \omega(q) \tag{S2}$$

Then we can obtain

$$\begin{aligned} \omega(\pi/a + \Delta q) &= \omega(-\pi/a - \Delta q) \\ &= \omega(-\pi/a - \Delta q + 2\pi/a) \\ &= \omega(\pi/a - \Delta q), \end{aligned} \tag{S3}$$

Furthermore, to have a finite and uniquely defined group velocity except at $q = 0$, the dispersion relation curve needs to be smooth, i.e.,

$$\omega'(q) \quad \text{is uniquely defined and bounded on } q \in (0, 2\pi/a) \tag{S4}$$

We note that the group velocity is doubly defined at $q = 0$ (and hence at $q = 2\pi/a, 4\pi/a, ...$, too) due to the direction flip, $\omega'(0_+) = -\omega'(0_-)$.
Next, combining Eqn. (S3) and (S4), we arrive at

$$\omega'(\pi/a) = \omega'(-\pi/a) = 0, \tag{S5}$$

which means the slope always vanishes at the Brillioun zone boundaries.
Next, free-standing systems without any elastic foundation of "grounded springs" do not admit any lower cut-off frequency. Consequently, we get

$$\omega(0) = 0. \tag{S6}$$

In addition, for the physical structure to be self-stable with a non-zero finite static stiffness, we also need to guarantee

$$0 < \omega'(0) < +\infty. \tag{S7}$$

To summarize, for any target dispersion relation $\Omega(q)$ defined on $q \in [0, \pi/a]$ to be physically possible, we need a *smooth* curve with

$$\Omega(0) = 0, \quad 0 < \Omega'(0) < +\infty, \quad \text{and} \quad \Omega'(\pi/a) = 0. \tag{S8}$$

MONO-ATOMIC SYSTEM FORMULATION

For a mono-atomic phononic chain with non-local springs up to N-th neighbor, we have the equation of motion for an arbitrary j-th mass in the chain as:

$$k_1(u_{j-1} - 2u_j + u_{j+1}) + k_2(u_{j-2} - 2u_j + u_{j+2}) + ... + k_N(u_{j-N} - 2u_j + u_{j+N}) = m\ddot{u}_j, \quad \text{(S9)}$$

where m and u_j are the mass and displacement, and k_n is spring constant for the nth-nearest neighbor interaction.

According to the Bloch theorem, the solution is in the following form:

$$u_j(t) = \hat{u}e^{i(jqa-\omega t)}, \quad \text{(S10)}$$

where t denotes time, $\hat{u}$ is the wave amplitude, i is the unit imaginary number, q is the (angular) wave number, a is the lattice constant, and ω is the (angular) frequency. Using Eqs. (S9) and (S10), we get

$$-m\omega^2 = k_1(2\cos(qa) - 2) + k_2(2\cos(2qa) - 2) + ... + k_N(2\cos(Nqa) - 2). \quad \text{(S11)}$$

The above equation can be simplified using $\cos(nqa) - 1 = -2\sin^2(\frac{nqa}{2})$, leading to

$$-m\omega^2 = -4k_1\sin^2(\frac{qa}{2}) - 4k_2\sin^2(\frac{2qa}{2}) - ... - 4k_N\sin^2(\frac{Nqa}{2}). \quad \text{(S12)}$$

Finally, we obtain the following dispersion relation

$$\omega(q) = 2\sqrt{\frac{k_1}{m}\sin^2(\frac{qa}{2}) + \frac{k_2}{m}\sin^2(\frac{2qa}{2}) + ... + \frac{k_N}{m}\sin^2(\frac{Nqa}{2})}. \quad \text{(S13)}$$

SINGLE-BAND SYSTEM DESIGN

The target curves in Figs. 2(a) and 2(b) in the main text are analytical functions:
For Fig. 2(a), we use

$$\omega(q) = \begin{cases} 3q\cos(0.6) & 0 \leq q \leq 0.2 \\ \sin(3q) + \omega(0.2) - sin(0.6) & 0.2 < q \leq 0.526 \\ \omega(q) = \omega(0.526) & 0.526 < q \leq 1 \end{cases} \tag{S14}$$

For Fig. 2(b), we use

$$\omega(q) = \begin{cases} 26.6q\cos(12.103) & 0 \leq q \leq 0.455 \\ \sin(26.6q) + \omega(0.455) - \sin(12.103) & 0.455 < q \leq 1 \end{cases} \tag{S15}$$

Hence, we can directly calculate the integration analytically with the functions listed above as the integrant.
Other target curves in the rest Fig. 2 of the main text are constructed using Bézier curves with different control points. Given $\beta+1$ control points $(P_0, P_1, ..., P_\beta)$, the Bézier curve can be defined as

$$\boldsymbol{B}(t) = \sum_{\alpha=1}^{\beta} b_\alpha^\beta(t) P_\alpha, \qquad 0 \leq t \leq 1 \tag{S16}$$

where $b_\alpha^\beta(t)$ is the Bernstein polynomial:

$$b_\alpha^\beta(t) = \frac{\beta!}{\alpha!(\beta-\alpha)!} t^\alpha (1-t)^{\beta-\alpha}. \tag{S17}$$

Therefore, by setting up multiple control points in Table I, we can obtain the arbitrary curves as shown in Fig. 2 in solid lines in the main text. Then, after capturing the data of the curves and following Eq. (4) and (5), we can calculate the parameters, k_n, as shown in Table II. For all cases, $m_1 = 1$.

Table I: Control points for the Bézier curve

Curve 2-c		**Curve 2-d**		**Curve 2-e**		**Curve 2-f**		**Curve 2-g**		**Curve 2-h**	
q	$\omega(q)$	q	$\omega(q)$	q	$\omega(q)$	q	$\omega(q)$	q	$\omega(q)$	q	$\omega(q)$
0	0	0	0	0	0	0	0	0	0	0	0
0.1	0.8	0.222	1.8134	0.0248	0.5876	0.0083	1.7096	0.0637	3.1752	0.1166	0.9728
0.2073	3.5707	0.1122	-0.2866	0.1382	0.1624	0.1688	5.5287	0.0554	1.6163	-0.1535	4.8115
0.7634	2.7024	0.778	0.6427	-0.0312	2.5611	0.314	1.7707	0.5312	-1.9994	0.4732	1.0446
0.3146	0.7902	0.222	2.1646	0.4427	1.1561	0.2564	-1.2232	-0.0038	-0.6083	-0.0006	-0.3618
1	0.9171	1	2.2411	0.249	1.2723	0.0873	0.4331	-0.1421	0.6331	-0.8525	0.936
				-0.1561	-1.942	0.7599	5.3758	0.62	2.6465	2.6052	1.223
				0.5662	-0.6758	0.5764	4.2548	0.2483	2.4819	-2.1446	3.0879
				0.4815	0.7659	0.337	-0.7415	-0.0198	1.3293	0.7408	2.8713
				-0.107	5.1051	0.3322	-5.2583	0.5669	-0.8045	0.8611	-1.5764
				0.6615	-1.7904	0.921	1.0806	0.9395	-0.3439	0.1745	-1.4427
				0.5166	0.4889	0.7395	7.2815	-0.0785	0.8079	1.2605	5.1554
				0.5898	2.5303	0.3115	4.2854	-0.3162	2.0255	-3.165	5.7758
				1	2.1162	1.0506	-2.2156	0.9427	4.7357	2.4414	0.2854
						0.794	2.1815	1.1529	2.8057	1.086	0.479
						0.921	2.379	0.2134	2.3694	-0.1465	1.6529
						1	2.2599	0.1299	-0.2783	-0.1064	-2.8739
								0.5223	-6.021	0.7235	0.1363
								0.4599	-1.0452	0.3204	0.7924
								2.0732	6.2166	0.393	1.9873
								-1.6663	0.873	-0.1229	3.1911
								3.1592	-0.9204	1.0159	3.8713
								-1	2.2134	-0.3538	1.6746
								1.5096	0.4108	2.6045	-1.2127
								1.0764	1.035	-0.749	0.7337
								0.5669	1.5892	0.1778	0.8372
								0.9624	1.7006	0.5045	-1.1573
								0.9854	2.0446	1.8605	0.0815
										0.6108	3.6955
										-0.2834	1.7401
										0.6294	1.8157
										1.6369	-1.2554
										0.3357	3.0076
										0.9399	1.3735
										0.8693	1.7922
										0.9728	2.2062

Table II: Final Design Parameters for Fig.2

k_n	**Fig.(a)**	**Fig.(b)**	**Fig.(c)**	**Fig.(d)**	**Fig.(e)**	**Fig.(f)**	**Fig.(g)**	**Fig.(h)**
k_1	0.195042	1.243081	-0.43158	1.2905	1.496408	0.01909	0.140741	0.06257
k_2	0.106402	0.58932	0.882255	-0.21601	-0.49976	-0.4717	-0.12216	-0.42643
k_3	0.027936	0.009712	0.588791	-0.14662	0.04535	0.14609	0.206253	0.111957
k_4	-0.00636	-0.1708	0.045147	0.106883	0.054588	0.397991	-0.14609	-0.11064
k_5	-0.00662	-0.04976	-0.00539	0.050975	-0.09066	0.275431	-0.04354	0.07046
k_6	0.000151	0.118901	0.081699	0.011358	0.107454	-0.01774	-0.05307	0.014392
k_7	0.000973	0.069273	0.042012	0.027031	0.132855	0.536803	0.102914	0.086872
k_8	-0.0008	-0.23849	-0.00894	0.01587	0.140528	0.186587	-0.01442	-0.06546
k_9	-0.00059	0.190481	0.005744	0.011387	0.067593	0.073902	5.23E-05	-0.00695
k_{10}	0.000501	-0.04681	0.018256	0.007145	0.012665	0.142534	0.036602	0.116466
k_{11}	0	0	0	0	-0.01686	0.097753	0.060161	0.12828
k_{12}	0	0	0	0	-0.01852	0.040082	0.067878	0.121427
k_{13}	0	0	0	0	-0.01129	0.074053	0.021871	0.104007
k_{14}	0	0	0	0	-0.00984	0.052984	0.021885	0.088381
k_{15}	0	0	0	0	-0.00817	0.012655	0.014445	0.075662
k_{16}	0	0	0	0	-0.00859	0.025735	0.016723	0.04871
k_{17}	0	0	0	0	-0.00193	0.024027	0.009909	0.04296
k_{18}	0	0	0	0	0.001704	0.009073	0.002757	0.035449
k_{19}	0	0	0	0	0.007099	0.009024	0.006728	0.042557
k_{20}	0	0	0	0	0.006733	0.014802	0.001365	0.034964
k_{21}	0	0	0	0	0	0	0	0.034095
k_{22}	0	0	0	0	0	0	0	0.026777
k_{23}	0	0	0	0	0	0	0	0.02541
k_{24}	0	0	0	0	0	0	0	0.017338
k_{25}	0	0	0	0	0	0	0	0.017458

TIME DOMAIN SIMULATIONS

As stated in the main text, to study the dynamical features of different critical points, we apply a time-dependent force at the left most mass of a finite chain. The forcing function is prescribed as a Gaussian envelop with the carrier-wave frequency corresponding to one of the critical points. Fig. S1 shows the forcing function we use for the second-order undulation (stationary inflection) point. The results of this input are plotted in Fig. 3(e) of the main text. The input excitations for results shown in Figs. 3(c) and 3(d) of the main text have the same form but different carrier frequencies.

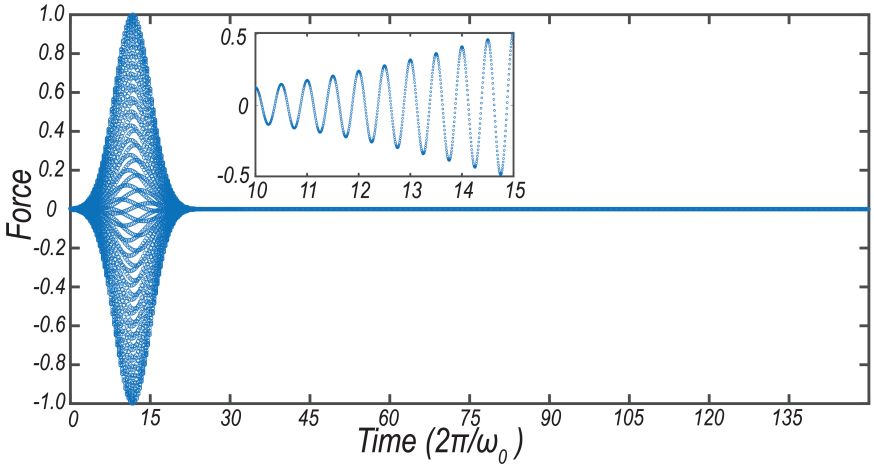

Figure S1. Gaussian pulse applied to the left-most mass to study the time domain response of a finite chain at the undulation-point frequency. The result of this input excitation is shown in Fig. 3(e) of the main text. Here $\omega_0 = \sqrt{k_1/m} = 1$.

DI-ATOMIC SYSTEM FORMULATION

A 2D schematic of the model is depicted in Fig. S2.

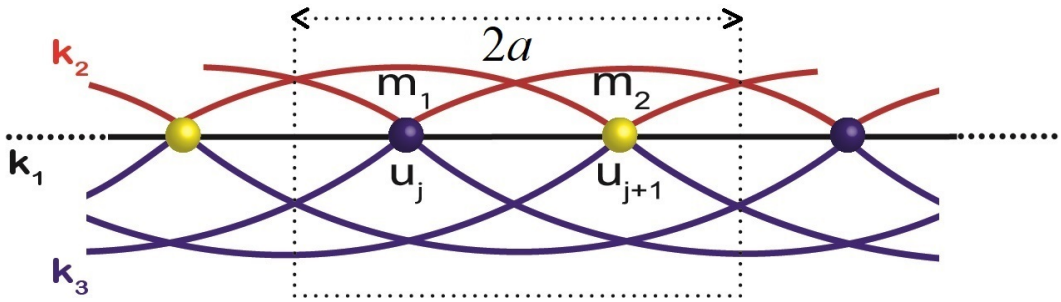

Figure S2. A non-local diatomic chain with the unit cell enclosed in the dashed rectangle. Each mass is connected to its nearest neighbors by linear springs with the spring constant k_1 (black lines). In addition, all masses are connected to their nth-nearest neighbors by linear springs with spring constants k_n. Red and blue lines represent second and third nearest non-local interactions, respectively.

For the case of di-atomic chain ($m_1 \neq m_2$), we can write the sum of spring forces for each masses to obtain the set of equations of motions.
For m_1 at the j-th position of the chain:

$$\begin{aligned} m_1\ddot{u}_j = {} & k_1(u_{j+1}-u_j) + k_2(u_{j+2}-u_j) + .. + k_N(u_{j+N}-u_j) \\ & + k_1(u_{j-1}-u_j) + k_2(u_{j-2}-u_j) + ... + k_N(u_{j-N}-u_j). \end{aligned} \tag{S18}$$

For m_2 at the $(j+1)$-th position of the chain:

$$\begin{aligned} m_2\ddot{u}_{j+1} = {} & k_1(u_{j+2}-u_{j+1}) + k_2(u_{j+3}-u_{j+1}) + .. + k_N(u_{j+1+N}-u_{j+1}) \\ & + k_1(u_j-u_{j+1}) + k_2(u_{j-1}-u_{j+1}) + ... + k_N(u_{j+1-N}-u_{j+1}). \end{aligned} \tag{S19}$$

We can write this set of equations in the matrix form of $\mathbf{M}\ddot{\boldsymbol{u}} + \mathbf{K}\boldsymbol{u} = 0$, where $\mathbf{M}$ and $\mathbf{K}$ are the mass and stiffness matrices, and $\boldsymbol{u}$ is the displacement vector.
Applying the Bloch theorem, we arrive at a two-degree-of-freedom system with

$$\mathbf{K} = \begin{bmatrix} \Lambda_0+\Lambda_1 & \Lambda_2 \\ \Lambda_3 & \Lambda_0+\Lambda_1 \end{bmatrix} \quad \text{and} \quad \mathbf{M} = \begin{bmatrix} m_1 & 0 \\ 0 & m_2 \end{bmatrix}, \tag{S20}$$

where

$$
\begin{aligned}
\Lambda_0 &= 2\sum_{n=1}^{N} k_n, \\
\Lambda_1 &= -2\sum_{\substack{n=2 \\ n \text{ even}}}^{N} k_n \cos(nqa), \\
\Lambda_2 &= -\sum_{\substack{n=1 \\ n \text{ odd}}}^{N} k_n (e^{i(n-1)qa} + e^{-i(n+1)qa}) = -e^{-iqa}\sum_{\substack{n=1 \\ n \text{ odd}}}^{N} k_n (e^{inqa} + e^{-inqa}) \\
&= -2e^{-iqa}\sum_{\substack{n=1 \\ n \text{ odd}}}^{N} k_n \cos(nqa), \\
\Lambda_3 &= -\sum_{\substack{n=1 \\ n \text{ odd}}}^{N} k_n (e^{-i(n-1)qa} + e^{i(n+1)qa}) = -e^{iqa}\sum_{\substack{n=1 \\ n \text{ odd}}}^{N} k_n (e^{-inqa} + e^{inqa}) \\
&= -2e^{iqa}\sum_{\substack{n=1 \\ n \text{ odd}}}^{N} k_n \cos(nqa).
\end{aligned}
\tag{S21}
$$

Solving $\mathbf{K} - \omega^2\mathbf{M} = 0$, we get the dispersion relations for both bands:

$$
\omega_{\mp}^2 = \frac{1}{2}(\Lambda_1 + \Lambda_0)(\frac{1}{m_1} + \frac{1}{m_2}) \mp \frac{1}{2}\sqrt{(\Lambda_1 + \Lambda_0)^2(\frac{1}{m_1} + \frac{1}{m_2})^2 + \frac{4}{m_1 m_2}(\Lambda_2\Lambda_3 - (\Lambda_1 + \Lambda_0)^2)},
\tag{S22}
$$

where $-$ and $+$ in the $\mp$ sign denote the first ("acoustic") and second ("optical") bands, respectively. Next, we define

$$
\begin{aligned}
K_0 &= \frac{1}{2}(\Lambda_0 + \Lambda_1) = \sum_{n=1}^{N} k_n - \sum_{\substack{n=2 \\ n \text{ even}}}^{N} k_n \cos(nqa), \\
K_1^2 &= \Lambda_2\Lambda_3 = \left(2\sum_{\substack{n=1 \\ n \text{ odd}}}^{N} k_n \cos(nqa)\right)^2, \\
\alpha &= m_2/m_1,
\end{aligned}
\tag{S23}
$$

with which Eq. (S22) becomes

$$
\begin{aligned}
\omega_{\mp}^2 &= K_0(\frac{1}{m_1} + \frac{1}{m_2}) \mp \sqrt{K_0^2(\frac{1}{m_1} + \frac{1}{m_2})^2 + \frac{1}{m_1 m_2}(K_1^2 - 4K_0^2)} \\
&= \frac{K_0}{m_1}(1 + \frac{1}{\alpha}) \mp \sqrt{(\frac{K_0}{m_1})^2(1 + \frac{1}{\alpha})^2 + \frac{1}{\alpha m_1^2}(K_1^2 - 4K_0^2)}
\end{aligned}
\tag{S24}
$$

Letting $m_1 = 1$, we arrive at

$$\omega_{\mp}^2 = K_0(1 + \frac{1}{\alpha}) \mp \sqrt{K_0^2(1 + \frac{1}{\alpha})^2 + \frac{1}{\alpha}(K_1^2 - 4K_0^2)} \tag{S25}$$

We can further define

$$\begin{aligned} A(q) &= \frac{\omega_+^2 + \omega_-^2}{2} = K_0(\frac{1}{m_1} + \frac{1}{m_2}) = \frac{\alpha + 1}{\alpha} K_0, \\ D(q) &= \frac{\omega_+^2 - \omega_-^2}{2} = \sqrt{[A(q)]^2 + \frac{1}{m_1 m_2}(K_1^2 - 4K_0^2)} = \sqrt{[A(q)]^2 + \frac{1}{\alpha}(K_1^2 - 4K_0^2)}. \end{aligned} \tag{S26}$$

DOUBLE-BAND SYSTEM DESIGN

We start with two arbitrarily smooth curves as the target dispersion relation, $\Omega_-(q)$ and $\Omega_+(q)$, defined over the positive half of the first Brillouin zone $q \in [0, \frac{\pi}{2a}]$. Here, the symmetry and physical requirements are

$$\begin{aligned} &\Omega_-(0) = 0, \quad 0 < \Omega'_-(0) < +\infty, \quad \Omega'_-(\frac{\pi}{2a}) = 0, \\ &0 < \Omega_+(0) < +\infty, \quad \Omega'_+(0) = 0, \quad \Omega'_+(\frac{\pi}{2a}) = 0. \end{aligned} \tag{S27}$$

and

$$0 \leq \Omega_-(q) \leq \Omega_+(q) \leq +\infty \quad \text{for} \quad q \in [0, \pi/(2a)] \tag{S28}$$

Since both dispersion curves directly scale with mass, we can always set, without loss of generality, $m_1 = 1$ and $\alpha = m_2/m_1 > 1$. Then, we use the following procedure to determine the $(N+1)$ design variables, $k_1, k_2, ...k_N$ and $\alpha = m_2/m_1$:
We first calculate

$$\begin{aligned} A(q) &= \frac{\Omega_+^2(q) + \Omega_-^2(q)}{2}, \\ D(q) &= \frac{\Omega_+^2(q) - \Omega_-^2(q)}{2}. \end{aligned} \tag{S29}$$

Next, we note

$$\frac{A(\frac{\pi}{2a})}{D(\frac{\pi}{2a})} = \frac{\Omega_+^2(\frac{\pi}{2a}) + \Omega_-^2(\frac{\pi}{2a})}{\Omega_+^2(\frac{\pi}{2a}) - \Omega_-^2(\frac{\pi}{2a})} = \frac{\alpha+1}{\alpha-1}, \tag{S30}$$

Then, we can obtain the mass ratio as

$$\frac{m_2}{m_1} = \alpha = \frac{\Omega_+^2(\frac{\pi}{2a})}{\Omega_-^2(\frac{\pi}{2a})}. \tag{S31}$$

We further calculate

$$K_0(q) = \frac{\alpha}{\alpha+1} A(q), \tag{S32}$$

$$K_1^*(q) = \sqrt{4K_0^2(q) - \alpha A^2(q) + \alpha D^2(q)}. \tag{S33}$$

In order for K_1^* to be real-valued, we need

$$4K_0^2(q) + \alpha D^2(q) \geq \alpha A^2(q). \tag{S34}$$

Plugging Eq. (S32) into Eq. (S34), we get

$$D^2(q) \geq \frac{(\alpha-1)^2}{(\alpha+1)^2} A^2(q). \tag{S35}$$

Based on Eqs. (S27) and (S28), we have $D(q) \geq 0$, $A(q) \geq 0$, and $\alpha > 1$. So, we arrive at

$$\frac{D(q)}{A(q)} = \frac{\Omega_+^2(q) - \Omega_-^2(q)}{\Omega_+^2(q) + \Omega_-^2(q)} \geq \frac{(\alpha-1)}{(\alpha+1)}. \tag{S36}$$

Therefore, to be realizable in a system of real-valued stiffness and mass variables, the target dispersion curves must also satisfy

$$\frac{\Omega_+(q)}{\Omega_-(q)} \geq \sqrt{\alpha} = \frac{\Omega_+(\frac{\pi}{2a})}{\Omega_-(\frac{\pi}{2a})}, \tag{S37}$$

i.e., the ratio between two bands, $\Omega_+(q)/\Omega_-(q)$, must reach its minimum value at $q = \pi/(2a)$. Hence, in addition to all requirements listed in Eqs. (S27) and (S28), for arbitrarily defined target curves, we also need to make sure the ratio between two bands, $R(q) = \Omega_+(q)/\Omega_-(q)$, satisfies

$$R(q) \geq R(\frac{\pi}{2a}) \quad \text{for} \quad q \in \Big(0, \frac{\pi}{2a}\Big). \tag{S38}$$

We note that this additional requirement Eq. S38 is only necessary if we want all mass and stiffness variables, m_1, m_2, k_1, k_2, ..., k_N, to be real-valued, which we desire for the simple examples presented in the main text. However, we can also go beyond this constraint if we allow complex-valued stiffnesses, which can be potentially realized through gain, loss, or gyroscopic effects in future studies.

As defined in Eq. (S33), K_1^* is positive, but our design protocol aims at taking the Fourier transform of a smooth function K_1. Therefore, we construct K_1 by changing the sign of K_1^* in the intervals between the roots of $K_1^* = 0$. We solve the equation $K_1^*(q) = 0$ to obtain its roots as $0 < q_1^* \leq q_2^* \leq q_3^* \leq ... \leq q_\eta^* < \frac{\pi}{2}$, where q_η^* is the largest root in the open interval of

$q \in \left(0, \frac{\pi}{2a}\right)$, and we define

$$K_1(q) = \begin{cases} K_1^*(q), & 0 \le q \le q_1^* \\ -K_1^*(q), & q_1^* < q \le q_2^* \\ K_1^*(q), & q_2^* < q \le q_3^* \\ ..., & ... \\ ..., & q_\eta^* < q \le \frac{\pi}{2} \end{cases} \tag{S39}$$

Lastly, we obtain all k_n's as

$$\begin{aligned} k_n &= \frac{2a}{\pi} \int_0^{\frac{\pi}{2a}} K_1 \cos(naq)\, \mathrm{d}q, \quad n = 1, 3, 5, ... \\ k_n &= -\frac{4a}{\pi} \int_0^{\frac{\pi}{2a}} K_0 \cos(naq)\, \mathrm{d}q, \quad n = 2, 4, 6, ... \end{aligned} \tag{S40}$$

Here, we would like to make some remarks about the important fact that this design protocol can customize each band individually without affecting the other band in the two-band system. This might be counter-intuitive at first glance, as changing any interaction should simultaneously affect both dispersion bands. However, we can better understand the independent-band-customization capability by the following logic: First, customizing each band individually is equivalent to customizing the square of each band individually since all frequencies are positive here. Then, it is also equivalent to independently customizing the sum and difference, i.e., $2A(q)$ and $2D(q)$, respectively, as defined in Eq. (S29). Next, by inspecting Eqs. (S32), (S33) and (S40) together, we note that while all k_n's affect $D(q)$, $A(q)$ is completely determined by even-index k_n's only. In conclusion, since the sum of the square of both bands solely depends on the even-index non-local interactions, we have enough "redundancy" or "orthogonality" to customize each of the two bands independently from each other.

For examples shown in Fig. 5 of main text, we use the following equations as the target dispersions for $qa \in [0, \pi/2]$.

For Fig. 5(a) in the main text,

$$\begin{cases} \Omega_- = \sin(qa), \\ \Omega_+ = 2. \end{cases} \tag{S41}$$

For Fig. 5(b) in the main text,

$$\begin{cases} \Omega_- = (41/2 - ((20(18\cos(3qa) + 2\cos(qa))^2)/21 + 3301/84)^{1/2})^{1/2}, \\ \Omega_+ = (((20(18\cos(3qa) + 2\cos(qa))^2)/21 + 3301/84)^{1/2} + 41/2)^{1/2}. \end{cases} \tag{S42}$$

For Fig. 5(c) in the main text,

$$\begin{cases} \Omega_- = \sqrt{\frac{\pi^2}{2} - (qa - \frac{\pi}{2})^2} - \frac{\pi}{2}, \\ \Omega_+ = 1.3 - 0.5\cos(4qa). \end{cases} \tag{S43}$$

For Fig. 5(d) in the main text,

$$\begin{cases} \Omega_- = -\cos[1.9(q + \pi/2/19)] + \cos(1.8\pi/2/19), \\ \Omega_+ = 2 - \cos(2q). \end{cases} \tag{S44}$$

The design parameters for Fig. 5 in the main text are shown in Table III.

Table III. Parameters of the designed systems shown in Fig. 5 of the main text

Fig. 5a		**Fig. 5b**		**Fig. 5c**		**Fig. 5d**	
$\alpha = 4.0$		$\alpha = 1.881$		$\alpha = 1.5118$		$\alpha = 2.2751$	
No.	k_n	*No.*	k_n	*No.*	k_n	*No.*	k_n
1	1.6	1	10	1	0.66	1	0.72
2	0.2	2	0	2	0.062	2	2.1
3	0.013	3	-2.9	3	-0.35	3	-0.39
4	0	4	0	4	0.4	4	-0.32
5	-5.1e-5	5	5.3	5	-0.18	5	0.014
6	0	6	0	6	0.0016	6	-4.0e-3
7	4.1e-7	7	1.8	7	0.06	7	-9.1e-4
8	0	8	0	8	-0.037	8	-9.3e-4
9	-3.7e-09	9	-0.33	9	0.01	9	-6.0e-4
10	0	10	0	10	0.00025	10	-3.4e-4
11	-5.9e-10	11	-0.82	11	-0.000078	11	-2.9e-4
12	0	12	0	12	0.00013	12	-1.5e-4
13	3.4e-10	13	-0.36	13	-0.000072	13	-1.5e-4
14	0	14	0	14	0.00007	14	-7.9e-5
15	-4.1e-10	15	0.19	15	0.00019	15	-8.1e-5
16	0	16	0	16	0.000041	16	-4.5e-5
17	1.6e-10	17	0.33	17	-0.000041	17	-4.8e-5
18	0	18	0	18	0.000026	18	-2.7e-5
19	1.2e-10	19	0.12	19	0.000064	19	-3.0e-5
20	0	20	0	20	0.000017	20	-1.8e-5

BAND DEGENERACIES

We recognize the importance of band degeneracies, such as Dirac-cone-like (i.e., locally linear) band crossings, which usually host rich physical features and unconventional properties in vibro-mechanical systems [1, 2, 3, 4]. To show the possibility of forming Dirac-cone-like degeneracies with the two-band design protocol, we conduct some additional parametric study on the di-atomic non-local chain by setting $m_1 = 1$ and $k_1 = 1$, while changing m_2, k_2, and k_3. The results are summarized in Fig. S3. We especially note that, while conventional local phononic crystals may host Dirac-cone-like degeneracies at either the boundary or center of the Brillouin zone, non-local phononic crystals can offer the additional features of forming Dirac-cone-like degeneracies at other locations in the Brillouin zone.

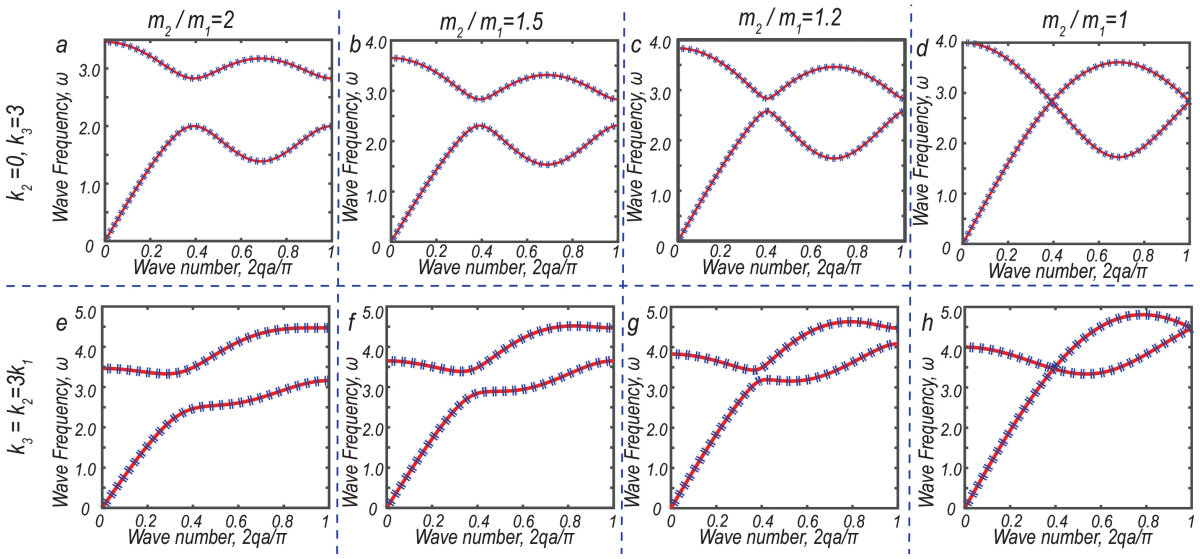

Figure S3. Additional parametric study on forming Dirac-cone-like degeneracies.

In addition, it is also possible to create higher-order (e.g. locally quadratic) band degeneracy in diatomic non-local phononic crystals. We show example cases for both linear and quadratic band degeneracies in the main text:

Linear crossings with $\alpha = 1, k_1 = 0.25$, and $k_2 = k_3 = 0.75$ in Fig. 5(e) of the main text.

Quadratic crossing with $\alpha = 1, k_1 = 0.9, k_2 = 0.6$, and $k_3 = 0.3$ in Fig. 5(f) of the main text.

NORMALIZED ROOT-MEAN-SQUARE DEVIATION (NRMSD)

We use the normalized root-mean-square deviation (NRMSD) to measure the differences between customized designs and the target dispersions. For this purpose, we first calculate the root-mean-square deviation (RMSD):

$$\mathrm{RMSD} = \sqrt{\frac{\sum_{i=1}^{T}(\omega_i - \omega_i^{\mathrm{target}})^2}{T}}, \tag{S45}$$

where T is the total number of data points, and we use $T = 3142$ in this study. Next, we normalize the RMSD by the band width,

$$\mathrm{NRMSD} = \frac{\mathrm{RMSD}}{\omega_{max} - \omega_{min}}. \tag{S46}$$

For multi-band systems, we further calculate the average NRMSD per band. The NRMSD for results shown in in Fig. 2 and Fig. 5 of the main text are provided in Table IV.

Table IV. Data of RMSD and NRMSD

Fig.2			**Fig.5**				
	RMSD	NRMSD		Lower bands		Upper bands	
Fig. 2a	0.002	0.000845		RMSD	NRMSD	RMSD	NRMSD
Fig. 2b	0.004	0.0016	*Fig. 5a*	1.96E-10	1.96E-10	4.83E-11	—
Fig. 2c	0.003	0.0014	*Fig. 5b*	0.019953	0.019953	0.0033661	0.017534
Fig. 2d	0.004	0.0016	*Fig. 5c*	0.00064073	0.00064073	0.000027317	0.00004917
Fig. 2e	0.004	0.002	*Fig. 5d*	0.00033482	0.00033504	0.000014066	0.000021099
Fig. 2f	0.012	0.005					
Fig. 2g	0.009	0.004					
Fig. 2h	0.022	0.0098					

TENTATIVE PHYSICAL DESIGN

There might be some potential concerns about the feasibility of non-local interactions. To address them, we present some drawings in Fig. S4, which can serve as compelling support for validating our theory experimentally. Although we drew a system with k_1 and k_3 only, we can also realize more sophisticated non-local phononic crystals with the same design approach, albeit with much more complex geometries.

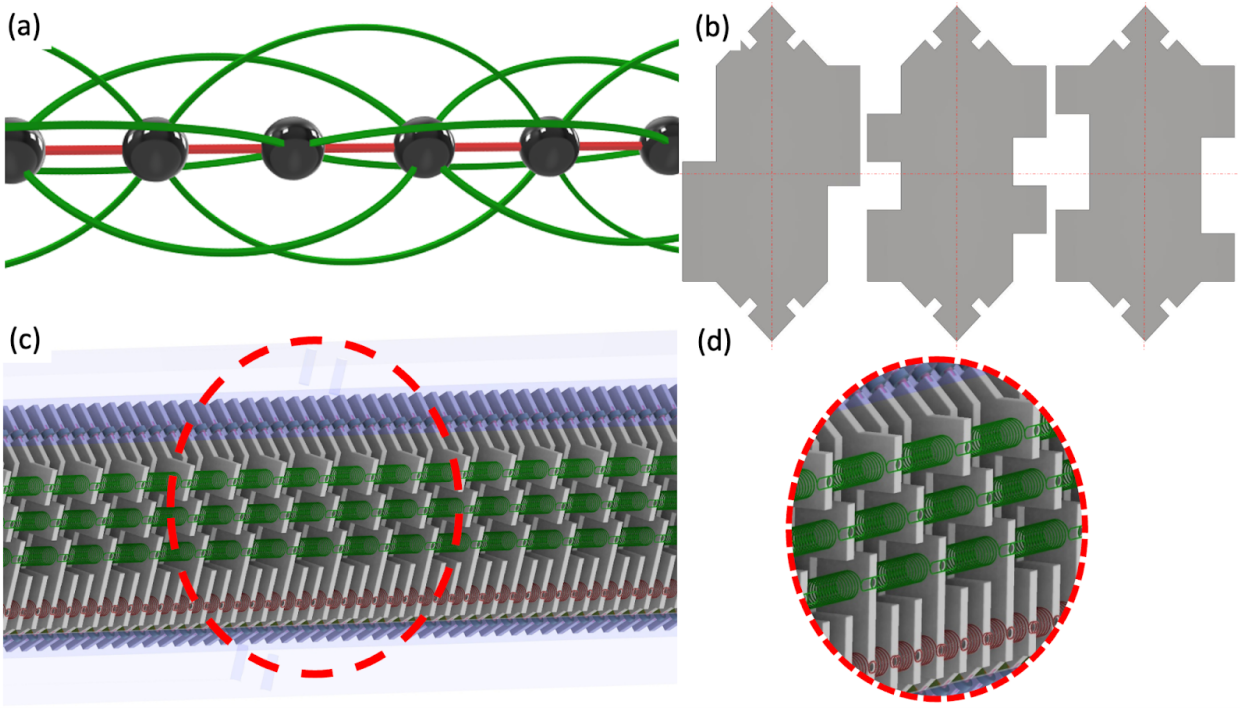

Figure S4. A tentative experimental implementation. (a) In the theoretical model of a 1D chain, all masses are the same, and there are two types of springs: k_1 and k_3. (b) To ensure that all springs k_1 and k_3 work independently without any interference, three types of blocks with different shapes but equal mass are used. We also make sure all mass blocks have the C_2 (180-degree-rotational) symmetry to minimize possible effects of excessive torque. (c) The experimental assembly depicts semi-transparent light-blue rails from above and below, and grey-colored mass blocks sandwiched between the two rails. The upper and lower ends of the mass blocks are equipped with rotary bearings to minimize friction. The springs k_1 and k_3 are depicted in red and green, respectively. (d) A zoom-in on a specific section of the assembly.

REFERENCES

[1] Maxime Lanoy et al. "Dirac cones and chiral selection of elastic waves in a soft strip". In: *Proceedings of the National Academy of Sciences* 117.48 (2020), pp. 30186–30190.

[2] AA Maznev. "Dirac cone dispersion of acoustic waves in plates without phononic crystals". In: *The Journal of the Acoustical Society of America* 135.2 (2014), pp. 577–580.

[3] Jun Mei et al. "First-principles study of Dirac and Dirac-like cones in phononic and photonic crystals". In: *Physical Review B* 86.3 (2012), p. 035141.

[4] Changqing Xu et al. "Three-dimensional acoustic double-zero-index medium with a fourfold degenerate Dirac-like point". In: *Physical Review Letters* 124.7 (2020), p. 074501.